

Journal of Materials Chemistry A

Accepted Manuscript



This is an *Accepted Manuscript*, which has been through the Royal Society of Chemistry peer review process and has been accepted for publication.

Accepted Manuscripts are published online shortly after acceptance, before technical editing, formatting and proof reading. Using this free service, authors can make their results available to the community, in citable form, before we publish the edited article. We will replace this *Accepted Manuscript* with the edited and formatted *Advance Article* as soon as it is available.

You can find more information about *Accepted Manuscripts* in the [Information for Authors](#).

Please note that technical editing may introduce minor changes to the text and/or graphics, which may alter content. The journal's standard [Terms & Conditions](#) and the [Ethical guidelines](#) still apply. In no event shall the Royal Society of Chemistry be held responsible for any errors or omissions in this *Accepted Manuscript* or any consequences arising from the use of any information it contains.



www.rsc.org/materialsA

Many-Body Interactions in Photo-Excited Lead Iodide Perovskite

M. Tuan Trinh, Xiaoxi Wu, Daniel Niesner, X.-Y. Zhu *

Department of Chemistry, Columbia University, New York, NY 10027, USA

* E-mail: xyzhu@columbia.edu

Abstract

Lead halide perovskite is emerging as a promising semiconductor material for thin film solar cells. Despite a large number of recent photophysical studies, the nature of photo-excitation in lead halide perovskite remains a subject of debate. Here we use transient absorption spectroscopy to re-examine lead halide perovskite thin films that have been reported to give the highest solar cell efficiencies. We focus on many-body interactions that are manifested in (1) the transient Stark effect exerted by hot carriers on subsequent e-h pair generation; and (2) the Auger recombination due to three-body carrier-carrier interactions. These observations establish the dominance of free carriers from above band-gap excitation in lead halide perovskite. We also suggest the effective dynamic screening of charge carriers, likely due to orientational freedom of methylamine cations in the perovskite lattice, and the presence of negligible charge carrier trapping in lead halide perovskite thin films grown in the presence of chloride precursors.

Lead iodide perovskite is emerging as a star material for low-cost photovoltaics,¹⁻⁷ thanks to the large optical absorption cross sections,⁸ long electron-hole diffusion lengths,^{9,10} and high carrier mobilities.^{11, 12} Such remarkable properties have motivated a large number of photophysical studies on lead halide perovskites, but the nature of photo-excitation across the bandgap remains a subject of debate.⁹⁻¹⁸ Support for the excitonic nature of excitation comes from exciton binding energy at or above thermal energy at room temperature^{13,15,19,20} and reports of high photoluminescence quantum yield and lasing in perovskites.^{8, 21 - 24} In contrast, experiments based on terahertz spectroscopy,¹² time-resolved photoluminescence,^{17, 25} and transient absorption spectroscopy^{14,21} suggest the free carrier nature. There are also reports on the dual nature of both free charge carriers and excitons.^{13,15} These debates have concerned mostly with band-gap excitations; even less is known about optical excitations with excess energy above the bandgap, i.e., “hot” excitations. Here we use femtosecond transient absorption (TA) spectroscopy to investigate many-body carrier-carrier interactions in lead iodide perovskites. We show that excitation above the bandgap results in free hot carriers that exert a transient Stark effect on subsequent optical excitations. Following the ultrafast cooling of hot carriers in ≤ 1 ps, we find the formation of predominantly band-edge carriers as population decay follows a third-order dependence on excitation density, in agreement with Auger recombination of free charge carriers, not excitons.

The samples used in this study were $\text{CH}_3\text{NH}_3\text{PbI}_3$ perovskite thin films obtained from dual source thermal evaporation in vacuum from $\text{CH}_3\text{NH}_3\text{I}$ and PbCl_2 precursors;⁴ details including X-ray diffraction analysis (Figure S1) can be found in supporting information (SI). Note that thin films grown from PbCl_2 have been called mixed halide perovskite, $\text{CH}_3\text{NH}_3\text{PbI}_{3-x}\text{Cl}_x$, but a

consensus arising from most recent experiments is that lead halide perovskites grown from both PbI_2 and PbCl_2 precursors possess similar structure and stoichiometry.^{26,27}

Figures 1A-C show pseudo-color ($-\Delta T/T$) representation of TA spectra as a function of probe wavelength and pump-probe delay with increasing excitation photon energy, $h\nu_1 =$ (A) 1.82 eV, (B) 2.95 eV, and (C) 3.88 eV. We observe two pronounced bleaching features at the optical bandgap of ~ 1.66 eV and at a higher energy of ~ 2.6 eV due to state-filling,⁹ and broad induced absorption in the range of 1.8-2.4 eV. In addition, there is a weak induced absorption feature at < 1.5 eV (obtained with an IR detector), as shown in Figure 1D for TA spectra at selected pump-probe delays. The decay of the induced absorption in the near-IR region corresponds to the rise in the visible induced absorption; both well described by single-exponential lifetimes of $\tau = 0.25 \pm 0.06$ ps, Figure 1E. This time constant is in excellent agreement with the hot carrier cooling time of $\tau = 0.24 \pm 0.02$ ps obtained from the growth of ground state bleaching at the same excitation energy, Figure 1F (detailed below). We assign the induced absorptions in the near-IR and visible ranges to intraband transitions from hot carriers and band-edge carriers, respectively. We also take the broad intraband absorption features as one of the evidences for free carrier characteristics,²⁸ not the discrete transitions expected from intraband excitonic transitions. Supporting evidences for free carriers come from the Stark effect and third-order Auger recombination rates, as detailed below.

We probe hot carrier cooling dynamics by varying the excitation photon energy and, thus, the initial excess carrier energy. The hot-carrier cooling rate can be calculated from the buildup of ground state bleaching probed at the bandgap energy. In order to remove the effect of red-shift (see below) on the buildup dynamics, we take integration over the spectral window (1.54-1.8 eV) covering the derivative peak around the bandgap.²⁹ The resulting buildup dynamics of the ground

state bleaching (normalized) at different excitation photon energies are shown in Figure 1F. The carrier cooling time (or band-edge population buildup time) is found to increase with pump photon energy, as expected from the transfer of more excess energy to the phonon bath at a higher excitation energy. In the measurement based on ground state bleaching, we cannot distinguish the cooling of the hot electron from that of the hot hole and obtained only an average rate. Given the similar effective masses of the electron and the hole in lead iodide perovskite³⁰ we expect that they possess similar cooling rates. We obtain hot carrier cooling time constants from single exponential fits to ground state recovery dynamics in Figure 1F. The resulting time constants are $\tau = 0.03 \pm 0.01$, 0.18 ± 0.02 , 0.24 ± 0.02 , 0.44 ± 0.04 ps, for $h\nu_1 = 1.82$, 2.25, 2.95, and 3.88 eV, respectively. The carrier cooling time is linearly related to the excess excitation energy ($h\nu_1 - E_g$), with an energy-loss rate, dE/dt , of 5.0 ± 0.4 eV/ps (Figure S2) for the dissipation of excess carrier energy to the phonon bath.

We now turn to a key feature in transient absorption spectra (Figures 1A-D) on the short time scale: the appearance of positive signal on the lower energy side of the band gap; this, along with the negative signal on the higher energy side, gives rise to a derivative peak shape at the band gap. The short-lived (< 1 ps) derivative peak is more obvious at higher photon energies (Figures 1A-C) and its dynamics correlate with that of hot carrier cooling, as shown by quantitative analysis below. A similar red-shift of the higher-lying band-band transition ~ 2.6 eV also gives rise to a derivative peak shape on the < 1 ps time scale. We assign these derivative features to spectral shifts in band-to-band transitions in the presence of hot carriers. In order to quantify spectral shift induced by the hot electron-hole pair, we carry out global fitting of transient absorption spectra, assuming that the band-edge absorption is described by a Gaussian function peaked at 1.656 eV as determined by the second derivative of the linear absorption spectrum (see

Figure S3). To minimize the number of variables, we restrain the width of the Gaussian peak as a global parameter. We perform global fits to TA spectra at various pump-probe delay times for $h\nu_1 = 1.82$ and 3.88 eV. Figure 2A shows three representative fits for $\Delta t = 0.1, 0.6,$ and 3 ps at $h\nu = 3.88$ eV. These fits yield spectral position as functions of Δt and $h\nu$. Figure 2B shows the magnitude of spectral red-shift in the presence of (hot) e-h at the two excitation photon energies, $h\nu = 1.82$ and 3.88 eV. The red-shift is the largest at the shortest time (higher excess energy) and amounts to 24 ± 2 meV for $h\nu_1 = 3.88$ eV, and 6 ± 1 meV for $h\nu_1 = 1.82$ eV. For both excitation energies, the red-shift decreases with increasing pump-probe delay and reaches a stable value of 3 ± 1 meV for $\Delta t > 1$ ps, as hot electrons/holes are cooled to the band-edges. The red-shifts decay on the sub-ps time scale, consistent with the hot carrier cooling times obtained from the growth of ground state bleaching (Figure 1F).

Further insight into the nature of spectral red-shifts comes from pump power dependence. As shown in Figure 3 for TA spectra at a pump-probe delay of 0.04 ps and different excitation laser power densities (0.8 - $10.8 \mu\text{J}/\text{cm}^2$), the magnitudes of the red-shift for both band-gap and the higher energy transitions are independent of excitation power density. This result indicates that the red-shift comes from two-body interactions between a photo-excited carrier with a transition generated by the probe pulse. Note that the pump power density used here is in the linear excitation region, as shown by the linear power dependence of total bleach signal for the band-gap excitation (averaged between 1.54 and 1.80 eV) for a pump-probe delay time of 2 ps, inset in Figure 3.

Optical excitation in semiconductors usually leads to a blue-shift in subsequent band-gap transitions. The blue-shift can result from band-filling (also called the Burstein-Moss effect)^{14,31,32} and screening of the excitonic resonance by existing carriers or excitons,³³⁻³⁵ all

these blue-shifts scale positively with excitation density,^{14,33-35} in contrast to the excitation power independent red-shift observed here during the lifetime of hot carriers. The observed red-shift in lead iodide perovskite can be understood as resulting from a transient Stark effect due to electric field from hot carriers. A bound Mott-Wannier exciton has no dipole moment and introduces no electric field, but a *free carrier* (electron or hole) does.^{29,36,37} For a dipole allowed optical transition, the shift in transition frequency, $\Delta\nu$, due to an electric field, $\vec{\epsilon}$, is given by³⁸

$$\Delta\nu = -\Delta\vec{\mu} \cdot \vec{\epsilon} - \frac{1}{2}\Delta\alpha \cdot |\vec{\epsilon}|^2 \quad (1)$$

where $\Delta\vec{\mu}$ and $\Delta\alpha$ are the changes in dipole moment and polarizability between the ground state and excited state of the material, respectively. The first term in equation (1) should result in a broadening in line shape due to the random orientation of $\Delta\vec{\mu}$ with respect to $\vec{\epsilon}$. The second term in equation (1) gives rise to a shift in the transition energy, with the sign of the shift given by the sign of $\Delta\alpha$. A red-shift in absorption means that the change in polarizability is positive, i.e. the excited state has higher polarizability than that of the ground state does. As shown in Figure 2B, the magnitude of red-shift scales with the excess energy of the photo-excited hot carrier and decreases with time as the hot carriers cool down, indicating that a carrier with more excess energy introduces higher electric field strength. This can be understood from the dynamic screening of the charge carrier. Given the ionic nature of the lead iodide crystal, particularly the freedom of motion of the methylamine cations, the local electric field produced by a free electron or hole can be effectively screened by the movements of ions.^{28,39-41} As a hot carrier cools, it is more effectively screened and becomes more “localized”, and therefore, the magnitude of Stark effect decreases; this can explain the scaling of observed red-shift with excess carrier energy, Figure 2B. Together with the broad induced absorption by hot carrier above, we conclude that photo excitation above the band-gap leads to the formation of free hot carriers.

Having addressed the role of hot carriers, we now turn to many-body interactions of band-edge carriers. For a semiconductor with sufficiently high excitation densities, non-radiative Auger recombination sets in. Auger recombination refers to the process in which an electron-hole pair across the band gap recombines non-radiatively by transferring the energy to a third particle, which can be an electron in the conduction band, a hole in the valence band, or an exciton.⁴² If the Auger process occurs between two excitons (also called exciton-exciton annihilation), the decay rate is given by:

$$\frac{dN}{dt} = -k_1N - k_A N^2 \quad (2)$$

where N is the number density of excitons; k_1 is the first-order rate constant for exciton recombination and k_A is the second-order rate constant for Auger recombination.

If the electrons and holes involved are treated as free carriers, the Auger recombination process follows a three-body collision model, i.e., electron-electron-hole or electron-hole-hole interaction. The rate equation can be written as:^{43,44}

$$\frac{dN}{dt} = -k_1N - k_2N^2 - k_A N^3 \quad (3)$$

where N is the number density of electrons or holes ($N = N_e = N_h$); k_1 is the first-order rate constant for single carrier trapping; k_2 is the second-order rate constant for radiative recombination; k_A is the third-order rate constant for Auger recombination. We note that equation (3) becomes indistinguishable from equation (2) when the Auger recombination channel is negligible.

Figure 4 shows the decay of ground state bleaching, integrated in the energy range of 1.54-1.8 eV, corresponding to the population decay of band-edge carriers or excitons. These band-

edge carriers or excitons are formed following picosecond relaxation of hot carriers from excitation at $h\nu = 2.95$ eV (see Figure 1E). The five sets of data span the range of 0.8-10.8 $\mu\text{J}/\text{cm}^2$ in excitation power density. While the initial signal (at $\Delta t = 2$ ps) scales linearly with excitation power density (see inset in Figure 3), the signal decay rate does not. The band-edge exciton/carrier decay dynamics can be described by the third order equation (equation 3) with universal kinetic parameters for all excitation laser power densities in the complete time window probed here, as shown by the good agreement between experimental data and fits in upper panel of Figure 4. In contrast, fits to the second order equation (equation 2) can only describe the population decay at the two lowest excitation densities, but clearly fails at high excitation power densities, lower panel in Figure 4.

The quantitative agreement between the excitation power-dependent decay dynamics and equation (3) establishes the predominantly free carrier nature of excited states in the lead iodide perovskite thin film. The discrepancy between equation (2) and experimental data in the lower panel of figure 4 becomes evident for a pump intensity of $3.2 \mu\text{J}/\text{cm}^2$, corresponding to an absorbed photon density of $1.1 \times 10^{18} \text{ cm}^{-3}$ (see section 5 in Supporting Information). The Auger recombination process, therefore, becomes competitive with radiative recombination only for charge carrier density $> 10^{18} \text{ cm}^{-3}$. The global fitting based on free carrier model yields a set of universal rate constants: $k_1 = 0$, $k_2 = 1.1 \times 10^{-9} \text{ cm}^3 \text{ s}^{-1}$, and $k_A = 3.8 \times 10^{-28} \text{ cm}^6 \text{ s}^{-1}$. The zero k_1 value reveals that single carrier trapping in the perovskite thin film grown from the PbCl_2 precursor is negligible. This result is in agreement with our recent spectroscopic study revealing negligible trap state density in this thin film⁴⁵ and previous reports of high solar cell performance.^{12, 46, 47} The second-order radiative recombination and the third-order Auger rate constants are in good agreement with the values reported by Saba et al.¹⁷ from a quantitative

analysis of photoluminescence decay dynamics and Wehrenfenning et al.¹² from THz spectroscopy.

The results and analysis presented here reveal two-types of many-body interactions in photo-excited lead iodide perovskite: (1) a Stark effect exerted by hot carriers on other across band-gap excitations; and (2) an Auger recombination process for band edge carriers at sufficiently high densities ($>10^{18}/\text{cm}^3$). In the former, we find that the transient electric field (and the associated Stark effect) almost vanishes as the hot carrier cools down (in $\sim 1\text{ps}$); this is consistent with the effective screening due to the orientational freedom of methylamine cations in the perovskite lattice. In the latter, we show that the decay of band-edge carriers can be quantitatively accounted for by second-order radiative recombination and third-order Auger recombination, with negligible first-order trapping to bandgap states.

Acknowledgements

X.Y.Z. acknowledges support by the US Department of Energy under grant No. ER46980. D. N. acknowledges support by the Deutsche Forschungsgemeinschaft (DFG Forschungsstipendium). Research carried out in part at the Center for Functional Nanomaterials, Brookhaven National Laboratory, which is supported by the U.S. Department of Energy, Office of Basic Energy Sciences, under contract number DE-AC02-98CH10886. We thank Matthew Y. Sfeir for technical help with transient absorption measurements.

References

- 1 Kojima, A.; Teshima, K.; Shirai, Y. Miyasaka, T. Organometal Halide Perovskites as Visible-Light Sensitizers for Photovoltaic Cells. *J. Am. Chem. Soc.* **2009**, 131, 6050–6051.
- 2 Kim, H. -S.; Lee, C. -R.; Im, J. -H.; Lee, K. -B.; Moehl, T.; Marchioro, A.; Moon, S. -J.; Humphry-Baker, R.; Yum, J.-H.; Moser, J. E.; Grätzel, M.; Park, N. -G. Lead Iodide Perovskite Sensitized All-Solid-State Submicron Thin Film Mesoscopic Solar Cell with Efficiency Exceeding 9%. *Sci. Rep.* **2012**, 2, 591-.
- 3 Lee, M. M.; Teuscher, J.; Miyasaka, T.; Murakami, T. N. Snaith, H. J. Efficient Hybrid solar Cells Based on Meso-Superstructured Organometal Halide Perovskites. *Science* **2012**, 338, 643–647.
- 4 Liu, M.; Johnston, M. B.; Snaith, H. J. Efficient Planar Heterojunction Perovskite Solar Cells by Vapour Deposition. *Nature* **2013**, 501, 395–398 (2013).
- 5 Hao, F.; Stoumpos, C. C.; Cao, D. H.; Chang, R. P. H.; Kanatzidis, M. G. Lead-Free Solid-State Organic–Inorganic Halide Perovskite Solar Cells. *Nat. Photonics* **2014**, 8, 489–494.
- 6 Burschka, J.; Pellet, N.; Moon, S.-J.; Humphry-Baker, R.; Gao, P. Nazeeruddin, M. K.; Grätzel, M. Sequential Deposition as a Route to High-Performance Perovskite-Sensitized Solar Cells. *Nature* **2013**, 499, 316–319.
- 7 Zhou, H.; Chen, Q.; Li, G.; Luo, S.; Song, T.-b.; Duan, H. –S.; Hong, Z.; You, J.; Liu, Y.; Yang, Y. Interface Engineering of Highly Efficient Perovskite Solar Cells. *Science*, **2014**, 345, 542-546.
- 8 Xing, G.; Mathews, N.; Lim, S. S.; Yantara, N.; Liu, X.; Sabba, D.; Grätzel, M.; Mhaisalkar, S.; Sum, T. C. Low-Temperature Solution-Processed Wavelength-Tunable Perovskites for Lasing. *Nat. Mater.* **2014**, 13, 476-480.
- 9 Xing, G.; Mathews, N.; Sun, S.; Lim, S. S.; Lam, Y. M.; Grätzel, M.; Mhaisalkar, S.; Sum, T. C. Long-Range balanced Electron- and Hole-Transport Lengths in Organic-Inorganic CH₃NH₃PbI₃. *Science* **2013**, 342, 344–347.
- 10 Stranks, D. S.; Eperon, G. E.; Grancini, G.; Menelaou, C.; Alcocer, M. J. P.; Leijtens, T.; Herz, L. M.; Petrozza, A.; Snaith, H. J. Electron-Hole Diffusion Lengths Exceeding 1

- Micrometer in an Organometal Trihalide Perovskite Absorber. *Science* **2013**, 342, 341–344.
- 11 Stoumpos, C. C.; Malliakas, C. D.; Kanatzidis, M. G. Semiconducting Tin and Lead Iodide Perovskites with Organic Cations: Phase Transitions, High Mobilities, and Near-Infrared Photoluminescent Properties. *Inorg. Chem.* **2013**, 52, 9019–9038.
- 12 Wehrenfennig, C.; Eperon, G. E.; Johnston, M. B.; Snaith, H. J.; Herz, L. M. High Charge Carrier Mobilities and Lifetimes in Organolead Trihalide Perovskites. *Adv. Mater.* **2014**, 26, 1584–1589.
- 13 D’Innocenzo, V.; Grancini, G.; Alcocer, M. J. P.; Kandada, A. R. S.; Stranks, S. D.; Lee, M. M.; Lanzani, G.; Snaith, H. J.; Petrozza, A. Excitons Versus Free Charges in Organolead Tri-halide Perovskites. *Nat. Commun.* **2014**, 5, 3586.
- 14 Manser, J. S.; Kamat, P. V. Band Filling with Free Charge Carriers in Organometal Halide Perovskites. *Nat. Photonics* **2014**, 8, 737–743.
- 15 Savenije, T. J.; Ponseca, C. S. Jr.; Kunneman, L.; Abdellah, M.; Zheng, K.; Tian, Y. Zhu, Q.; Canton, S. E.; Scheblykin, I. G.; Pullerits, T.; Yartsev, A.; Sundström, V. Thermally Activated Exciton Dissociation and Recombination Control the Carrier Dynamics in Organometal Halide Perovskite. *J. Phys. Chem. Lett.* **2014**, 5, 2189–2194.
- 16 Stranks, S. D.; Burlakov, V. M.; Leijtens, T.; Ball, J. M.; Goriely, A.; Snaith, H. J. Recombination Kinetics in Organic-Inorganic Perovskites: Excitons, Free Charge, and Subgap States. *Phys. Rev. Appl.* **2014**, 2, 034007.
- 17 Saba, M.; Cadelano, M.; Marongiu, D.; Chen, F.; Sarritzu, V.; Sestu, N.; Figus, C.; Aresti, M.; Piras, R.; Lehmann, A. G.; Cannas, C.; Musinu, A.; Quochi, F.; Mura, A.; Bongiovanni, G. Correlated Electron-Hole Plasma in Organometal Perovskites. *Nat. Commun.* **2014**, 5, 5049.
- 18 Ponseca, C. S. Jr.; Savenije, T. J.; Abdellah, M.; Zheng, K.; Yartsev, A.; Pascher, T.; Harlang, T.; Chabera, P.; Pullerits, T.; Stepanov, A.; Wolf, J. -P.; Sundström, V. Organometal Halide Perovskite Solar Cell Materials Rationalized: Ultrafast Charge Generation, High and Microsecond-Long Balanced Mobilities, and Slow Recombination. *J. Am. Chem. Soc.* **2014**, 136, 5189–5192.

- 19 Tanaka, K.; Takahashi, T.; Bana, T.; Kondo, T.; Uchida, K.; Miura, N. Comparative Study on The Excitons in Lead-Halide-Based Perovskite-Type Crystals $\text{CH}_3\text{NH}_3\text{PbBr}_3$ $\text{CH}_3\text{NH}_3\text{PbI}_3$. *Solid State Commun.* **2003**, 127, 619–623.
- 20 Sun, S.; Salim, T.; Mathews, N.; Duchamp, M.; Boothroyd, C.; Xing, G.; Sum, T. C.; Lam, Y. M. The Origin of High Efficiency in Low-Temperature Solution-Processable Bilayer Organometal Halide Hybrid Solar Cells. *Energy Environ. Sci.* **2014**, 7, 399–407.
- 21 Deschler, F.; Price, M.; Pathak, S.; Klintberg, L. E.; Jarausch, D. -D.; Högler, R.; Hüttner, S.; Leijtens, T.; Stranks, S. D.; Snaith, H. J.; Atatüre, M. Phillips, R. T.; Friend, R. H. High Photoluminescence Efficiency and Optically Pumped Lasing in Solution-Processed Mixed Halide Perovskite Semiconductors. *J. Phys. Chem. Lett.* **2014**, 5, 1421–1426 .
- 22 Tan, Z.-K.; Moghaddam, R. S.; Lai, M. L.; Docampo, P.; Högler, R.; Deschler, F.; Price, M.; Sadhanala, A.; Pazos, L. M.; Credgington, D.; Hanusch, F.; Bein, T.; Snaith, H. J.; Friend, R. H. Bright Light-Emitting Diodes Based on Organometal Halide Perovskite. *Nat. Nanotechnol.* **2014**, 9, 687–692.
- 23 Sutherland, B. R.; Hoogland, S.; Adachi, M. M.; Wong, C. T.; Sargent, E. H. Conformal Organohalide Perovskites Enable Lasing on Spherical Resonators. *ACS Nano* **2014**, 8, 0947–10952
- 24 Zhang, Q.; Ha, S. T.; Liu, X.; Sum, T. C.; Xiong, Q. Room-Temperature Near-Infrared High-q Perovskite Whispering-Gallery Planar Nanolasers. *Nano Lett.* 2014, 14, 5995–6001.
- 25 Yamada, Y.; Nakamura, T.; Endo, M.; Wakamiya, A.; Kanemitsu, Y. Photocarrier Recombination Dynamics in Perovskite $\text{CH}_3\text{NH}_3\text{PbI}_3$ for Solar Cell Applications. *J. Am. Chem. Soc.* **2014**, 136, 11610–11613.
- 26 Grätzel, M. The Light and Shade of Perovskite Solar Cells. *Nat. Mater.* 2014, 13, 838–842.
- 27 Dar, M. I.; Arora, N.; Gao, P.; Ahmad, S.; Grätzel, M.; Nazeeruddin, M. K. Investigation Regarding the Role of Chloride in Organic-Inorganic Halide Perovskites Obtained from Chloride Containing Precursors. *Nano Lett.* **2014**, 14, 6991–6996.
- 28 Even, J.; Pedesseau, L.; Katan, C. Analysis of Multivalley and Multibandgap Absorption and Enhancement of Free Carriers Related to Exciton Screening in Hybrid Perovskites. *J. Phys. Chem. C* **2014**, 118, 11566–11572..

-
- 29 Trinh, M. T.; Sfeir, M. Y.; Choi, J. J.; Owen, J. S.; Zhu, X. -Y. A Hot Electron-Hole Pair Breaks the Symmetry of A Semiconductor Quantum Dot. *Nano Lett.* **2013**, *13*, 6091–6097.
- 30 Giorgi, G.; Fujisawa, J.; Segawa, H.; Yamashita, K. Small Photocarrier Effective Masses Featuring Ambipolar Transport in Methylammonium Lead Iodide Perovskite: A Density Functional Analysis. *J. Phys. Chem. Lett.* **2013**, *4*, 4213–4216.
- 31 Burstein, E. Anomalous optical absorption limit in InSb. *Phys. Rev.* **1954**, *93*, 632–633.
- 32 Moss, T. S. The interpretation of the properties of indium antimonide. *Proc. Phys. Soc. B* **1954**, *67*, 775–782.
- 33 Peyghambarian, N.; Gibbs, H.; Jewell, J.; Antonetti, A.; Migus, A.; Hulin, D.; Mysyrowicz, A. Blue Shift of the Exciton Resonance due to Exciton-Exciton Interactions in a Multiple-Quantum-Well Structure. *Phys. Rev. Lett.* **1984**, *53*, 2433–2436.
- 34 Wachter, S.; Maute, M.; Kalt, H.; Galbraith, I.; Sieh, C.; Meier, T.; Koch, S. W. Excitation Induced Shift and Broadening of the Exciton Resonance. *Phys. B Condens. Matter* **2002**, *314*, 309–313.
- 35 Manzke, G.; Peng, Q.; Henneberger, K.; Neukirch, U.; Hauke, K.; Wundke, K.; Gutowski, J.; Hommel, D. Density Dependence of the Exciton Energy in Semiconductors. *Phys. Rev. Lett.* **1998**, *80*, 4943–4946.
- 36 Cappel, U. B.; Feldt, S. M.; Schöneboom, J.; Hagfeldt, A.; Boschloo, G. The Influence of Local Electric Fields on Photoinduced Absorption in Dye-Sensitized Solar Cells. *J. Am. Chem. Soc.* **2010**, *132*, 9096–101.
- 37 Roiati, V.; Mosconi, E.; Listorti, A.; Colella, S.; Gigli, G.; De Angelis, F. Stark Effect in Perovskite/TiO₂ Solar Cells: Evidence of Local Interfacial Order. *Nano Lett.* **2014**, *14*, 2168–2174.
- 38 Bublitz, G. U.; Boxer, S. G. Stark Spectroscopy: Applications in Chemistry, Biology, and Materials Science. *Annu. Rev. Phys. Chem.* **1997**, *48*, 213–242.
- 39 Juarez-Perez, E. J.; Sanchez, R. S.; Badia, L.; Garcia-Belmonte, G.; Kang, Y. S.; Mora-Sero, I.; Bisquert, J. Photoinduced Giant Dielectric Constant in Lead Halide Perovskite Solar Cells. *J. Phys. Chem. Lett.*, **2014**, *5*, 2390-2394.

-
- 40 Lin, Q.; Armin, A.; Nagiri, R. C. R.; Burn, P. L.; Meredith, P.; Electro-optics of perovskite solar cells. *Nat. Photon.* **2014**, doi:10.1038/nphoton.2014.284
- 41 Even, J.; Pedesseau, L.; Katan, C. Analysis of multivalley and multibandgap absorption and enhancement of free carriers related to exciton screening in hybrid perovskites. *J. Phys. Chem. C* **2014**, *118*, 11566-11572.
- 42 Landsberg, P. *Recombination in Semiconductors* (Cambridge Univ. Press, Cambridge, **1991**).
- 43 Yamada, Y.; Yasuda, H.; Tayagaki, T.; Kanemitsu, Y. Photocarrier Recombination Dynamics in Highly Excited SrTiO₃ Studied by Transient Absorption and Photoluminescence Spectroscopy. *Appl. Phys. Lett.* **2009**, *95*, 121112.
- 44 Trinh, M. T.; Limpens, R.; Gregorkiewicz, T. Experimental Investigations and Modeling of Auger Recombination in Silicon Nanocrystals. *J. Phys. Chem. C* **2013**, *117*, 5963–5968.
- 45 Wu, X.; Trinh, M. T.; Niesner, D.; Zhu, H.; Norman, Z.; Owen, J. S., Yaffe, O., Kudisch, B. J.; Zhu, X.-Y. *J. Am. Chem. Soc.* **2015**, *137*. DOI: 10.1021/ja512833n
- 46 Colella, S.; Mosconi, E.; Fedeli, P.; Listorti, A.; Gazza, F.; Orlandi, F.; Ferro, P.; Besagni, T.; Rizzo, A.; Calestani, G.; Gigli, G.; De Angelis, F.; Mosca, R. MAPbI₃-xCl_x Mixed Halide Perovskite for Hybrid Solar Cells: The Role of Chloride as Dopant on the Transport and Structural Properties. *Chem. Mater.* **2013**, *25*, 4613–4618.
- 47 Zhao, Y.; Zhu, K. CH₃NH₃Cl-Assisted One-Step Solution Growth of CH₃NH₃PbI₃: Structure, Charge-Carrier Dynamics, and Photovoltaic Properties of Perovskite Solar Cells. *J. Phys. Chem. C* **2014**, *118*, 9412–9418.

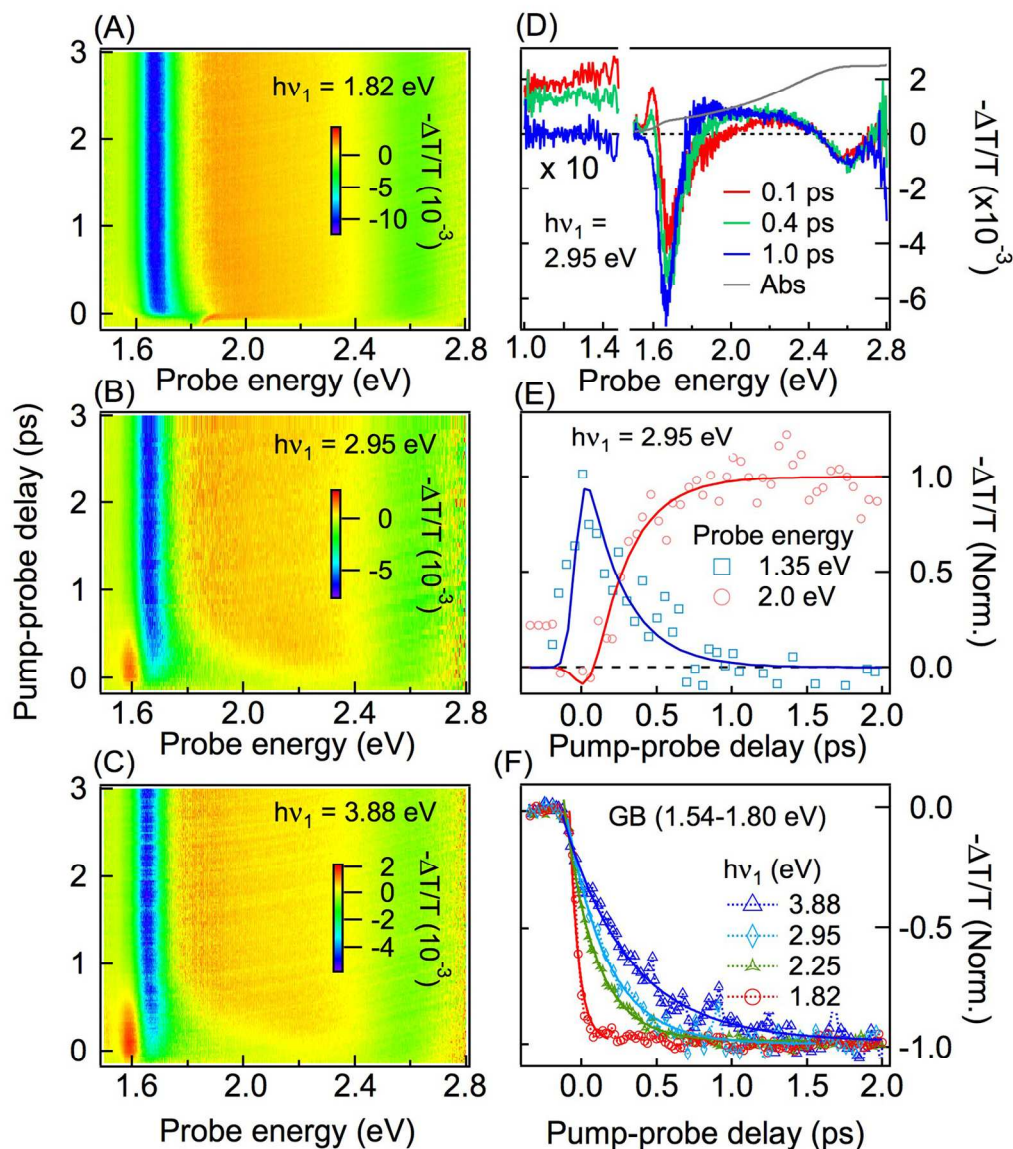


Figure 1. Pseudo-color ($-\Delta T/T$) representation of TA spectra at three excitation photon energies, $h\nu_1$: (A) 1.82 eV, (B) 2.95 eV, and (C) 3.88 eV. (D) Transient absorption spectra for $h\nu_1 = 2.95$ eV in the near IR ($\times 10$) and visible regions at short delay times (red: 0.1 ps; green: 0.4 ps; blue: 1.0 ps). Also shown in panel (D) is a linear absorption spectrum (grey). (E) Normalized TA signals probed below (1.35 eV) and above (2 eV) bandgap as a function of pump-probe delay. (F) Normalized buildup of bleaching signal for different excitation energies $h\nu_1 = 3.88$ eV (blue), 2.95 eV (light blue), 2.25 eV (green), and 1.82 eV (red). In each case, the signal (color symbols) was integrated in a probe photon energy window of 1.54-1.80 eV. The solid lines are single-exponential fits (convoluted with laser pulses). All measurements were performed at room temperature.

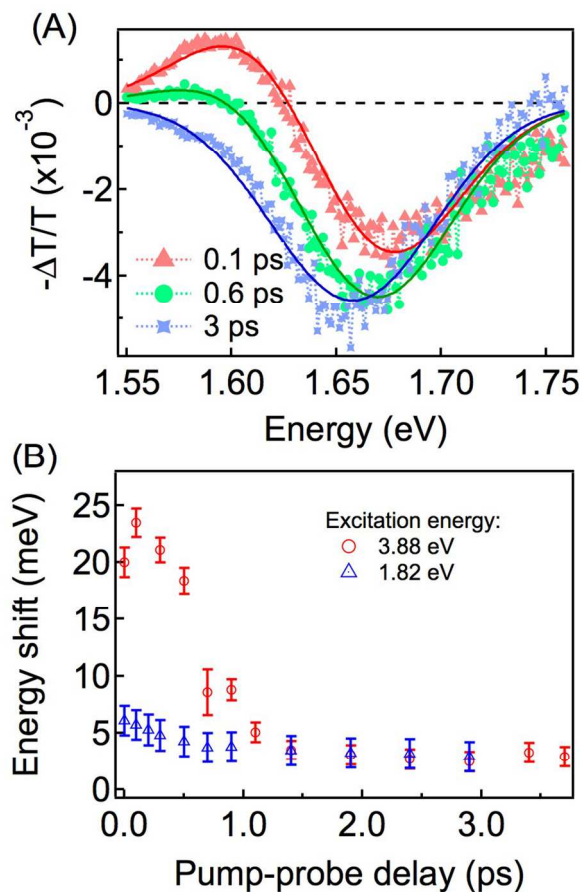


Figure 2. (A) Global fits to transient absorption spectra at different delay times for 3.88 eV excitation, for clarity only three curves are shown. The excitation density is $1.9 \mu\text{J}/\text{cm}^2$ (B) Energy red-shifts as a function of pump-probe delay obtained from global fits for two excitation photon energies.

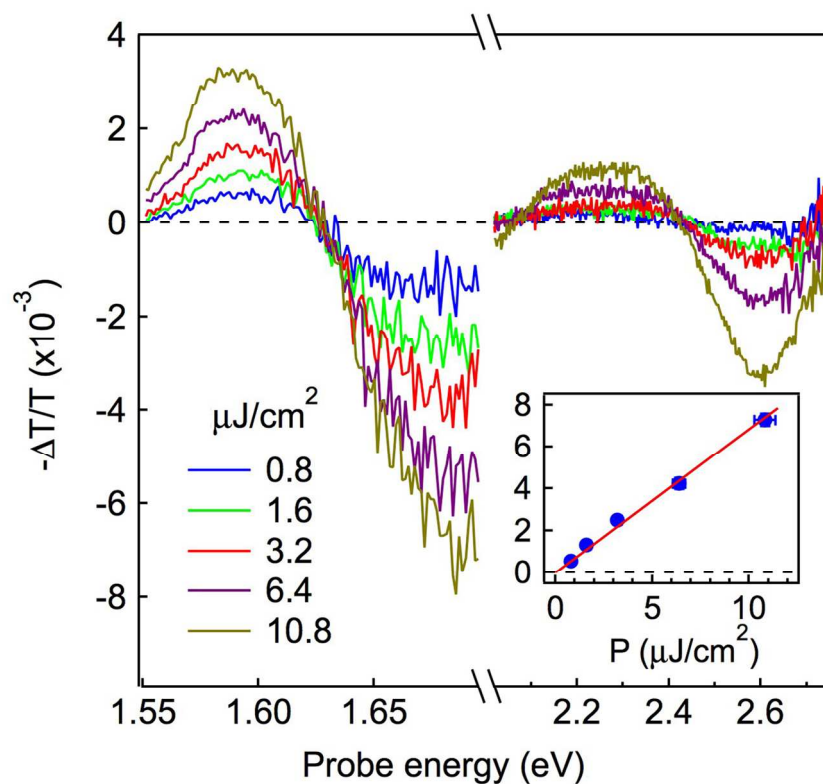


Figure 3. Transient absorption spectra at a pump-probe delay of 0.04 ps for different excitation laser pulse energy densities (0.8-10.8 $\mu\text{J}/\text{cm}^2$) at an excitation photon energy of $h\nu_1 = 2.95$ eV. The inset shows the bandgap bleaching signal (dots, integrated in the probe photon energy window of 1.54-1.80 eV) as a function of excitation laser pulse energy density (P , $\mu\text{J}/\text{cm}^2$). The solid line is a linear fit.

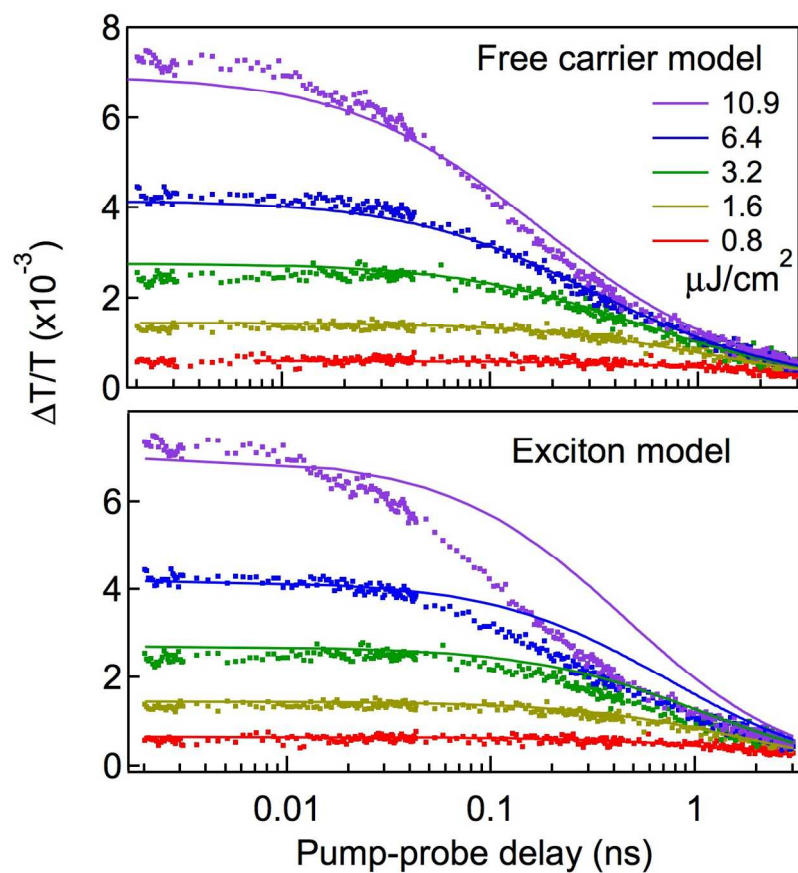
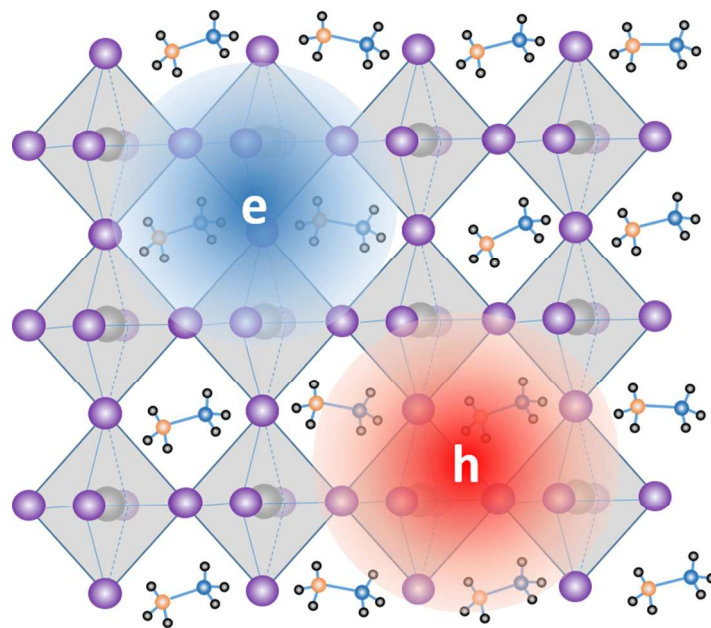


Figure 4. Band-edge bleaching dynamics at different excitation densities (dots) and global fits (solid lines) based on the 3-body Auger model (upper panel) and the 2-body exciton Auger model (lower panel). The data traces (dots) are averaged in the probe window of 1.54-1.8 eV. All measurements at room temperature.



TOC figure